

BEL-Float

Survivability assessment of FOWTs

Deliverable D1.1.2.1. – Open-source numerical model useful for survivability assessment of FOWT

Date of delivery: 12/10/2026

Authors: Yuki Igarashi, Annelie Baines-Maitland, Maximilian Streicher and Peter Troch

University: Ghent University

Faculty: Faculty of Engineering and Architecture

Department: Department of Civil Engineering

Email: yuki.igarashi@ugent.be

Financially supported by the FPS Economy (FOD Economie) under the call 2022 of the Energy Transition Fund.

Contents

1 BEL-Float Project....2
2 Introduction....2
3 Numerical method....3
3.1 DualSPHysics - MoorDyn+ model....3
3.2 Lumped–mass model (LM)....4
4 Numerical Model Setup....5
4.1 DualSPHysics Configuration....5
4.2 Validation and Convergence Study....7
4.2.1 Wave elevation....8
4.2.2 Heave response and resolution sensitivity....9
4.2.3 Mooring line segments sensitivity test....9
5 Simulation Results....10
5.1 Focused wave simulations with varying peak period....10
6 Conclusion....11
Acknowledgements....12
References....12

The sole responsibility for the content of this document lies with the author(s). It does not necessarily reflect the opinion of the FOD Economy – Directory of Energy, and does not make them responsible for any use that may be made of the information contained therein.

1 BEL-Float Project

The main goal of the BEL-Float project is to be a catalyst for the Belgian offshore wind sector in the field of floating offshore wind, to ensure and strengthen its top position as an industrial world player in offshore energy expertise and know-how, by prominently putting floating offshore wind on the academic research agenda. The two main objectives are to create an innovation backbone through innovation and knowledge building by compiling and absorbing research expertise from our Norwegian academic partners, initiating new and innovative research, setting up a future research and development roadmap, and to provide a skilled workforce by developing a training and skills-building program, which will be perpetuated in a series of structural advanced floating offshore wind courses.

As part of the BEL-Float projects and topic 2: Survivability in extreme sea states, the following tasks is defined:

1. Develop a numerical model based on Smoothed Particle Hydrodynamics (SPH), including the coupled effects of hydrodynamic loads and the mooring lines.
2. Accurately model the Floating Offshore Wind (FOW) system in extreme sea states to assess the platform's survivability and dynamic response.
3. Set up an experimental campaign using a scaled model of an FOW with mooring lines. The resulting dataset will be used for validation of the developed numerical model.

This document presents Deliverable D1.1.2.1. Open-source numerical model useful for survivability assessment of FOW turbines.

2 Introduction

Floating offshore wind turbines (FOWTs) are increasingly recognized as a viable solution for harnessing renewable energy in offshore regions. Commercial projects are now targeting deeper sites that reach the limit for installing fixed-bottom offshore wind turbines, which is around 70–100 m water depth. When transitioning to FOWTs, the mooring system becomes a critical design focus, as platform motions are highly sensitive to hydrodynamic loading that can strongly amplify line tensions. Many of the concepts proposed in this water depth range rely on semi-submersible platforms supported by catenary mooring systems, which operate under different hydrodynamic and mooring constraints compared with similar platforms deployed in deep water [1].

In intermediate water depths, mooring system behaviour becomes strongly nonlinear. As the catenary mooring lines have limited space to hang, small platform motions can lead to large variations in line tension. During platform motion, specific local segments of the mooring line transition between taut and slack states and may produce sudden changes in effective stiffness that cause tension spikes [2]. Meanwhile, under energetic wave conditions, drag forces become increasingly important in the hydrodynamic loading acting on the mooring lines [3, 4]. These effects tightly couple platform motion and mooring response, making the mooring system an active and highly nonlinear component.

A critical effect commonly discussed in relation to this nonlinearity is snap loading. Snap loads are defined as loads that arise when a mooring line transitions from a slack or near-slack state to a highly tensioned state over a very short time interval [5]. Slack formation is often associated with platform motions that reduce effective line tension, while rapid re-tensioning generates a sharp tensile disturbance that propagates along the line as an axial stress wave [6, 7]. The relatively limited catenary curve in intermediate water depths leads to rapid stress-wave reflections and pronounced high-frequency tension oscillations, which are superimposed on the low-frequency platform response [8]. Thus, snap loading plays a key role in both fatigue and extreme load design. Repeated slack–taut transitions have been shown to significantly accelerate fatigue damage in mooring chains [9, 10], and peak snap tensions may exceed the mooring chain maximum breaking load over a very short duration,

The sole responsibility for the content of this document lies with the author(s). It does not necessarily reflect the opinion of the FOD Economy – Directory of Energy, and does not make them responsible for any use that may be made of the information contained therein.

raising concerns for ultimate strength and safety margins [11]. These characteristics make snap loads a governing limit state for mooring systems supporting FOWTs in intermediate water depths.

Despite extensive research, accurately predicting snap loads remains challenging for commonly used numerical models. Lumped-mass mooring solvers are widely applied in engineering practice due to their computational efficiency and have been validated against experimental data for floating wind platforms [12]. However, their spatial discretisation and numerical damping can limit their ability to resolve fast axial stress-wave propagation. As a result, snap loads may be smoothed or misrepresented, leading to underestimation or overestimation of peak tensions [13, 14]. Even with advanced numerical approaches such as high-order finite-element methods (FEM), capturing snap loads still requires careful treatment of wave propagation and numerical stability and remains computationally demanding [11]. These limitations indicate that the reliability of snap load prediction is still strongly model-dependent and requires further study.

Besides the mooring line model itself, the accuracy of extreme sea state hydrodynamics is also a critical component for reliable snap load prediction. Recently, particle-based fluid solvers based on Smoothed Particle Hydrodynamics (SPH) have gained attention for simulating highly nonlinear free-surface flows and fluid–structure interaction. SPH naturally captures large deformations and violent impact phenomena [15, 16]. The open-source SPH solver, DualSPHysics, is capable of modelling multiphysics problems such as floating structures and their interactions with ocean waves and mooring lines [17, 18]. Recent studies have demonstrated that SPH-based simulations can reproduce the wave-induced response of semi-submersible FOWT platforms with good agreement against experimental measurements [19]. By leveraging the coupling of DualSPHysics with the dynamic mooring solver, MoorDyn+, it provides a good platform for investigating, in depth, snap loading under extreme sea states and for systematically identifying the limitations of conventional mooring line models in intermediate water depths.

3 Numerical method

3.1 DualSPHysics - MoorDyn+ model

This study employs the high-fidelity coupled model integrating DualSPHysics and MoorDyn+. DualSPHysics is a high-fidelity open-source code that uses SPH for engineering problems involving free-surface hydrodynamics [17, 20]. SPH is a mesh-free, Lagrangian method that discretizes the fluid domain into particles carrying mass, momentum, and other physical properties. By updating the particle position based on the Navier-Stokes equations of momentum and continuity, SPH is well suited for simulations characterised by large deformations, free surfaces, and multiphase interactions as it allows the free evolution of particles without restrictions from a background mesh [17]. In DualSPHysics, the interaction of each particle is evaluated over neighbouring particles located inside the compact support of the smoothing kernel, which is defined by the smoothing length h. In this way, field variables are approximated through kernel interpolation, and the governing equations are transformed into particle summations that can be solved explicitly in time [20].

The fluid dynamics are governed by the discrete momentum equation for a particle a interacting with neighbouring particles b [15]:

$$\frac{d v_a}{d t} = -\sum_b m_b \left(\frac{P_a}{\rho_a^2} + \frac{P_b}{\rho_b^2} + \Pi_{ab} \right) \nabla_a W_{ab} + g \tag{1}$$

where P and ρ denote pressure and density, Π_{ab} is the artificial viscosity term ensuring numerical stability during shock events, and W_{ab} is the smoothing kernel function. Solving this equation explicitly allows the model to capture highly nonlinear hydrodynamic pressure fields acting on the hull

The sole responsibility for the content of this document lies with the author(s). It does not necessarily reflect the opinion of the FOD Economy – Directory of Energy, and does not make them responsible for any use that may be made of the information contained therein.

without the filtering effects inherent in potential flow solvers. In DualSPHysics, the particle density is evolved from the SPH continuity equation,

$$\frac{d\rho_a}{dt} = \sum_b m_b (v_a - v_b) \cdot \nabla_a W_{ab}, \tag{2}$$

while the pressure is obtained using a weakly compressible equation of state of the Tait form,

$$P_a = B\left[\left(\frac{\rho_a}{\rho_0}\right)^{\gamma} - 1\right], \tag{3}$$

where ρ_0 is the reference density, γ is the polytropic constant, and $B = c_0^2 \rho_0 / \gamma$ depends on the artificial speed of sound c_0 [20]. This weakly compressible treatment is selected in DualSPHysics so that density variations remain small while keeping the time step computationally practical. In addition, DualSPHysics includes a density diffusion term in the continuity equation to reduce spurious high-frequency density oscillations caused by the stiff equation of state, particle disordering and the WC nature of the formulation. In the present work, this stabilization is introduced through the Fourtakas Density Diffusion Term, which is implemented in DualSPHysics as a correction of the standard density diffusion formulation [20].

For the solid boundaries and floating body interaction, DualSPHysics represents the geometry using boundary particles. In the standard Dynamic Boundary Condition (DBC), these particles satisfy the same governing equations as fluid particles but remain fixed or move according to an imposed motion, generating a repulsive pressure response as fluid particles approach the boundary. In the modified Dynamic Boundary Condition (mDBC), ghost nodes are projected into the fluid across the boundary interface in order to improve the near-wall pressure and velocity treatment and reduce the excessive dissipation associated with the original DBC formulation [20]. mDBC is particularly useful for the present floating-body problem, where accurate local pressure transfer from the fluid to the rigid platform is required.

The structural response of the mooring system is solved simultaneously using the MoorDyn+ module. Coupling is achieved through a bi-directional communication scheme executed at every time step [21, 20]. The SPH solver computes the instantaneous rigid body motion of the floating platform and passes the fairlead kinematic state, which is the position and velocity, to the mooring solver. MoorDyn+ then computes the dynamics of each node i along the line according to Newton's second law as defined in Eq. (4). The resulting tension vector at the fairlead node is fed back into the SPH solver as an external force acting on the rigid body to close the dynamic loop. In the DualSPHysics–MoorDyn implementation, this exchange follows a loose two-way coupling strategy: the platform motions are first passed from DualSPHysics to MoorDyn, MoorDyn solves the mooring response over the DualSPHysics time step, and the updated fairlead forces are then returned to DualSPHysics and added to the rigid-body force balance [20, 21].

3.2 Lumped–mass model (LM)

The lumped–mass (LM) formulation implemented in MoorDyn+ represents a mooring line as a discrete system of point masses connected by axially deformable segments [12, 22]. Structural mass is lumped at the nodes, while the connecting segments transmit axial load without distributed inertia along the segment length. LM model neglected bending stiffness, torsional stiffness, and rotational inertia, and the mooring line is treated as a perfectly flexible cable. Under these assumptions, the dynamic response of the line arises from nodal translation driven by axial tension, hydrodynamic loading, and gravity.

The sole responsibility for the content of this document lies with the author(s). It does not necessarily reflect the opinion of the FOD Economy – Directory of Energy, and does not make them responsible for any use that may be made of the information contained therein.

For a node i with position vector $r_i(t) \in \mathbb{R}^3$, the governing equation of motion follows directly from Newton's second law:

$$(m_i + a_i)\ddot{r}_i(t) = T_{i+\frac{1}{2}} - T_{i-\frac{1}{2}} + W_{sub,i} + D_{n,i} + D_{t,i} + B_i, \tag{4}$$

where m_i denotes the nodal structural mass and a_i the hydrodynamic added mass. The submerged weight $W_{sub,i}$ accounts for gravity and buoyancy. Hydrodynamic drag forces $D_{n,i}$ and $D_{t,i}$ are evaluated using Morison-type formulations and applied at the nodes [3, 4]. The seabed reaction force B_i is modelled as a unilateral vertical spring–damper contact force activated when node elevation falls below the seabed level [22].

Internal force transmission is governed by the segment geometry. For the segment connecting nodes i and $i+1$, the displacement vector $d_{i+\frac{1}{2}} = r_{i+1} - r_i$ defines the instantaneous segment length $L_{i+\frac{1}{2}} = \| d_{i+\frac{1}{2}} \|$ and the unit tangent direction $\hat{t}_{i+\frac{1}{2}} = d_{i+\frac{1}{2}} / L_{i+\frac{1}{2}}$. While $l_{0,i+\frac{1}{2}}$ denoting the unstretched segment length, the axial engineering strain is

$$\varepsilon_{i+\frac{1}{2}} = \frac{L_{i+\frac{1}{2}} - l_{0,i+\frac{1}{2}}}{l_{0,i+\frac{1}{2}}}. \tag{5}$$

The LM formulation in MoorDyn assumes a linear spring–damper for axial deformation of each segment [22, 23]. Segment tension is determined by axial strain and strain rate, with compressive response suppressed so that only tension is transmitted.

$$T^{LM}_{i+\frac{1}{2}} = \begin{cases} EA_0 \varepsilon_{i+\frac{1}{2}} + C_A \dot{\varepsilon}_{i+\frac{1}{2}}, & \varepsilon_{i+\frac{1}{2}} > 0, \\ 0, & \varepsilon_{i+\frac{1}{2}} \le 0. \end{cases} \tag{6}$$

which EA_0 is a constant axial stiffness and C_A is a constant axial damping coefficient.

The LM model captures geometric nonlinearity associated with large displacements and reorientation of the mooring line. Variations in catenary shape, loss and recovery of tension, and slack–taut transitions arise naturally through continuous updates of segment length and direction [2]. As a result, snap events caused by sudden geometric re-engagement can occur within the model, and the discretized line may exhibit wave-like axial transients that contribute high-frequency tension components [5, 6, 7]. Material nonlinearity is not included, as the axial response is modeled using a linear stiffness and damping law [9]. The assumption of constant stiffness EA_0 removes strain-hardening effects, and the linear damping term cannot reproduce rate-dependent stiffness or asymmetric loading–unloading behaviour, so snap loading is represented primarily through geometric effects and a linear rate term in the current model[10, 8]. These modelling assumptions impose intrinsic limitations on snap-load prediction.

4 Numerical Model Setup

4.1 DualSPHysics Configuration

The fluid is modeled with a reference density of $\rho_0 = 1025\,kg/m^3$, while pressure stability is enhanced using the Fourtakas Density Diffusion Term (DDT) with a coefficient of 0.1. Fluid–structure

The sole responsibility for the content of this document lies with the author(s). It does not necessarily reflect the opinion of the FOD Economy – Directory of Energy, and does not make them responsible for any use that may be made of the information contained therein.

interaction and solid boundaries are treated using the mDBC with a free-slip formulation. The main SPH numerical parameters are summarized in Table 1.

Table 1: Summary of SPH numerical configuration.

Parameter	Value
Reference density, ρ_0	$1025\,kg/m^3$
Particle spacing, dp	$0.75\,m$
Smoothing length, h	$1.5\,m$
Kernel function	Wendland
δ_{DDT}	0.1
Viscosity treatment	Laminar
Boundary method	mDBC
Slip mode	Free-slip
Time integration scheme	Symplectic

The numerical wave tank extends from $x=-150\,m$ to $500\,m$ in the wave propagation direction and has a width of $240\,m$, as shown in Figure 1. A long sloping region starting at $x=120\,m$ until $x=500\,m$ is implemented as a relaxation zone to suppress wave reflection. A uniform water depth of $70\,m$ is adopted to represent intermediate-depth conditions before the start of the sloping region. Waves are generated using a piston-type wavemaker driven by second-order wavemaker theory. The main domain and wave-generation settings are summarized in Table 2.

Extreme wave conditions are generated by producing a $+x$ direction crest-focused wave group embedded in a JONSWAP spectrum with a peak enhancement factor of $\gamma=3.3$. The target sea state corresponds to a significant wave height of $H_s=12\,m$ and a peak period of $T_p=8\,s$, with the theoretical focus location set at $x_f=70\,m$ from the wavemaker.

Table 2: Summary of the numerical wave tank and focused-wave generation settings.

Parameter	Value
Tank width	$240\,m$
Still water depth	$70\,m$
Wavemaker type	Piston-type
Wave generation theory	Second-order
Spectrum	JONSWAP
Peak enhancement factor, γ	3.3
Number of wave components	512
Target significant wave height, H_s	$12\,m$
Focus location, x_f	$70\,m$
Initial ramp time	$32\,s$
Final ramp time	$30\,s$

The floating structure is the OC4-DeepCwind semi-submersible platform, modeled as a rigid body with a total mass of $1.3473\times10^7\,kg$, and the main platform and mooring properties are summarized in Table 3. Six-degree-of-freedom platform motion is resolved using Project Chrono and coupled with the SPH solver. The mooring system consists of three catenary mooring lines modeled in MoorDyn+.

The sole responsibility for the content of this document lies with the author(s). It does not necessarily reflect the opinion of the FOD Economy – Directory of Energy, and does not make them responsible for any use that may be made of the information contained therein.

Fairlead and anchor horizontal coordinates follow the standard OC4 definition [24], while Line 1, which is aligned with the x-axis and facing the wave, is the main observed mooring line.

To maintain the target pretension at a water depth of $70\,m$ from the OC4 definition, the unstretched mooring line length is reduced to $801.8\,m$. Each mooring line has a constant axial stiffness of $EA = 7.536 \times 10^8\,N$.

Table 3: Platform and mooring system properties used in the present model.

Component	Parameter	Value
Platform	Mass	1.3473×10^7 kg
	I_x, I_y	6.827×10^9 kg·m²
	I_z	1.226×10^{10} kg·m²
	Motion solver	Project Chrono
	Chrono time step	$0.01\,s$
Mooring	Number of lines	3
	Line length	801.8 m
	Segments per line	180
	Stiffness (EA)	7.536×10^8 N
	Diameter (d)	0.0766 m
	Linear mass	113.35 kg/m
	Fairlead depth	-14.0 m
	Anchor depth	-70 m

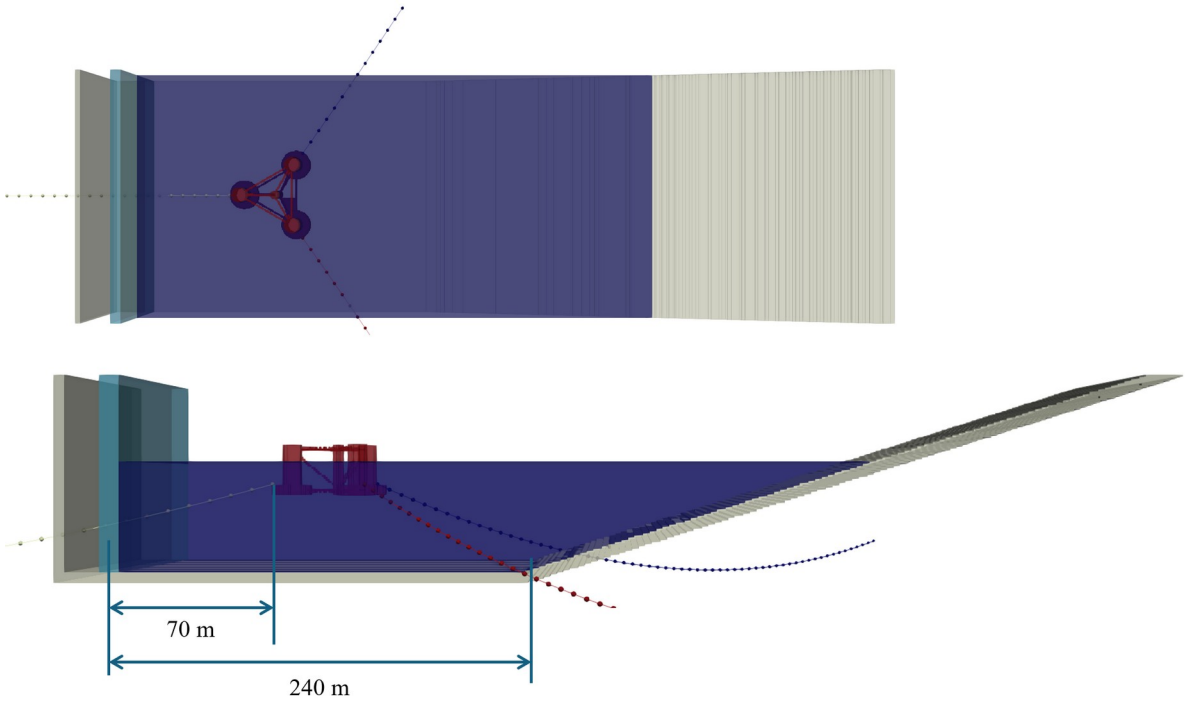


Figure 1: Numerical model setup showing the OC4-DeepCwind platform in the SPH wave tank. The domain includes a piston-type wavemaker and a uniform water depth of $70\,m$ before the sloping region. The mooring system preserves the standard OC4 footprint, with the line length adjusted to $801.8\,m$ in the present model.

4.2 Validation and Convergence Study

A convergence study was performed using focused-wave simulations with varying particle spacing $d\,p$ to assess the sensitivity of wave generation and platform dynamic response to spatial

The sole responsibility for the content of this document lies with the author(s). It does not necessarily reflect the opinion of the FOD Economy – Directory of Energy, and does not make them responsible for any use that may be made of the information contained therein.

discretization, and the reliability of the model was further validated by reproducing the OC4 reference case at a water depth of 200 m.

4.2.1 Wave elevation

Wave generation accuracy was evaluated using a focused wave event with wave height $H = 12\,m$ and period $T = 8.5\,s$, with a focused-wave ramp time of $32\,s$. The free-surface elevation at the theoretical focus location x_f for three spatial resolutions, $dp = 1.5\,m$, $1.0\,m$, and $0.75\,m$, was similar across the three resolutions.

The theoretical profile of the wave in this model is based on New Wave theory, which describes a focused wave group as the deterministic superposition of spectral components that are phased to concentrate at a selected focus position and time. The underlying sea state is described by a JONSWAP spectrum, so the focused wave group can be interpreted as a New Wave event constructed from a JONSWAP spectral distribution. This is suitable for this study because the JONSWAP spectrum was originally developed from measurements obtained during the Joint North Sea Wave Project and is widely used to represent sea states associated with the North Sea. Thus, the focused wave is used to simulate an extreme sea condition by representing the most critical wave event embedded within the prescribed irregular sea state [25].

The free-surface elevation produced in the model could be written as

$$\eta(x,t) = \frac{A}{\sigma^2}\sum_{i=1}^{N} S_{\eta\eta}(\omega_i)\cos\left[k_i(x - x_f) - \omega_i(t - t_f) + \phi\right]\Delta\omega, \tag{7}$$

where $S_{\eta\eta}(\omega_i)$ is the wave spectral density, ω_i is the angular frequency of the i-th component, k_i is the corresponding wavenumber, x_f and t_f are the theoretical focus location and focus time, ϕ is the phase at focus, σ^2 is the variance of the sea state, and A is the target linear focus amplitude. Therefore, the New Wave profile provides the theoretical reference for the present focused-wave validation.

Figure 2 compares the surface elevation for the target resolution, $dp = 0.75\,m$, against the corresponding New Wave theory profile and shows that, for the target resolution $dp = 0.75\,m$, the crest elevation fit well with the New Wave theory, while the troughs before and after the main crest do not fit very well. This behaviour is consistent with observations reported in the DualSPHysics documentation. All three resolutions reproduce the focused wave group, show similar results, and reach a wave height close to the prediction from New Wave theory. Overall, all dp values reproduce the phase evolution of the focused wave group, while the $dp = 0.75\,m$ case is selected as the target resolution for the subsequent simulations.

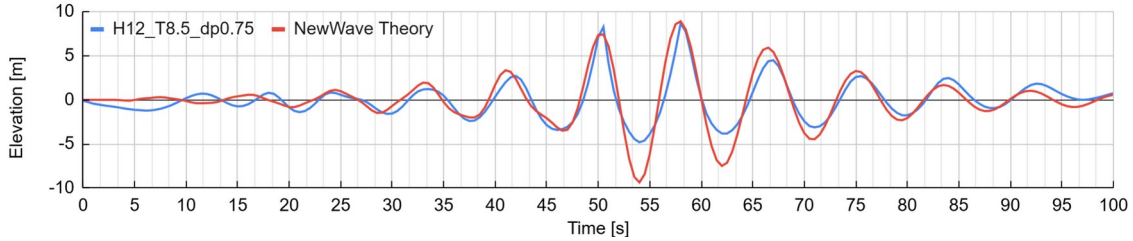


Figure 2: Free-surface elevation at the focus location $x = -40\,m$ for a focused wave ($H = 12\,m$, $T = 8.5\,s$) for the $dp = 0.75\,m$ case, compared with the corresponding New Wave theory profile.

The sole responsibility for the content of this document lies with the author(s). It does not necessarily reflect the opinion of the FOD Economy – Directory of Energy, and does not make them responsible for any use that may be made of the information contained therein.

4.2.2 Heave response and resolution sensitivity

The sensitivity of platform rigid-body dynamics to SPH spatial discretization was further examined through heave decay simulations. Figure 3 presents the heave response for different particle spacings, together with a validation against a reference OC4 case.

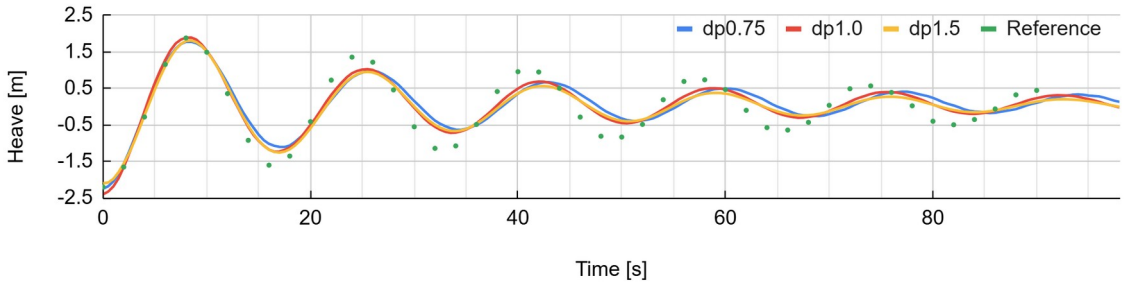


Figure 3: Heave response of the OC4 platform for three SPH particle spacings ($d\,p = 1.50$, 1.00, and $0.75\,m$), compared with the OC4 reference solution at 200 m water depth.

Figure 3 compares the heave response obtained with $d\,p = 0.75\,m$ against the reference OC4 solution at a water depth of $200\,m$. The numerical result captures the first oscillation cycle well. From the second cycle onward, the heave response shows stronger damping than the reference solution, leading to progressively smaller amplitudes and a gradual phase drift over time. A mismatch in oscillation period relative to the reference solution is also apparent. These differences indicate that the free-decay response in the present SPH model is not yet fully captured. The lower oscillation amplitude may also lead to underprediction of platform motion, associated nonlinear response and mooring tension, which need to be taken into consideration when interpreting the subsequent simulation results. Overall, the $d\,p = 0.75\,m$ case shows the most consistent response among the tested resolutions and is selected as the baseline resolution for subsequent extreme sea state simulations, with some uncertainty in platform motion remaining. A more detailed investigation of the free-decay behaviour in SPH, including the source of the observed damping and period discrepancies, is still needed and will form part of the next phase of this work.

4.2.3 Mooring line segments sensitivity test

The discretization of the mooring line is also a critical parameter that needs to be validated to confirm the accuracy of the predicted mooring tension. In a lumped-mass mooring model, too few mooring segments may smooth the transient tension response and lead to inaccurate peak prediction under focused-wave excitation.

To validate the mooring tension captured in the model using the mentioned settings,, a benchmark case with 400 segments was taken as the reference, and additional simulations were performed with 60, 120, and 180 segments under the same focused-wave condition. As shown in Figure 4, the 60- and 120-segment cases underpredict the peak tension response, while the 180-segment case shows close agreement with the 400-segment case. Therefore, 180 segments are considered sufficient for the present study, considering both accuracy and computational cost.

The sole responsibility for the content of this document lies with the author(s). It does not necessarily reflect the opinion of the FOD Economy – Directory of Energy, and does not make them responsible for any use that may be made of the information contained therein.

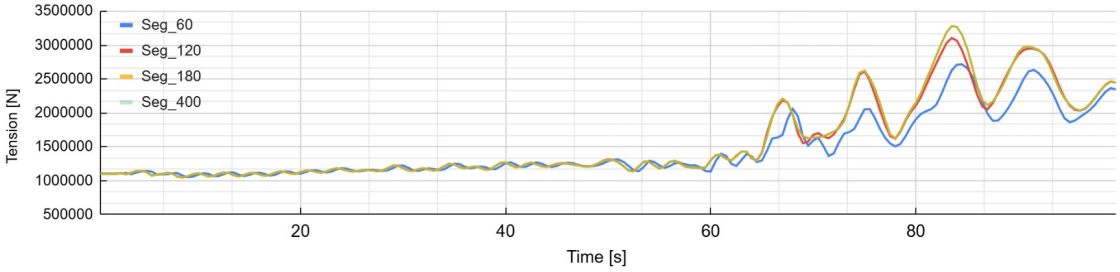


Figure 4: Comparison of mooring tension time histories obtained using different numbers of mooring line segments under the same focused-wave condition. The 180-segment case shows close agreement with the 400-segment benchmark, while the 60- and 120-segment cases underpredict the peak tension response.

5 Simulation Results

5.1 Focused wave simulations with varying peak period

Figure 5 presents the time histories of the free surface elevation at the focus location, which is right before interacting with the mooring fairlead, and the corresponding fairlead tension of Line 1 for a single crest-focused wave group with target wave height $H = 12\,m$. Peak wave periods of $T = 8$, 10, 12, and 14 s are examined, while all other numerical and physical parameters remain unchanged. All simulations were performed on the HPC-UGent Tier-2 infrastructure using the joltik GPU cluster, and each simulation required approximately 17 h of simulation time.

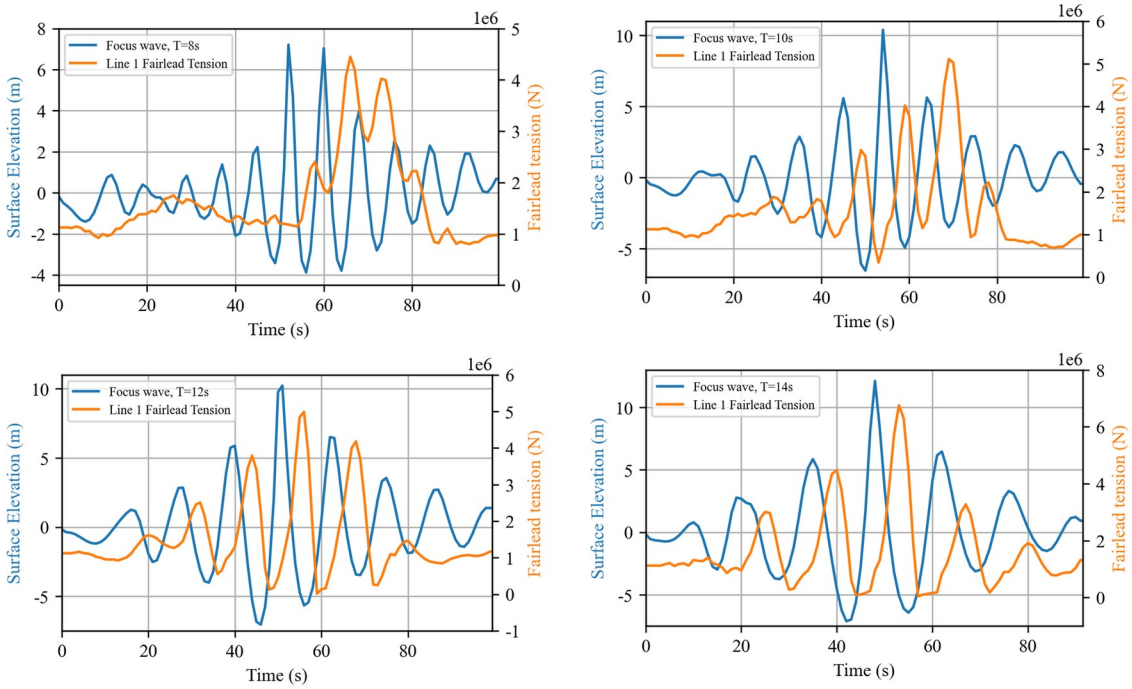


Figure 5: Time histories of free surface elevation at the focus location and fairlead tension of Line 1 for crest-focused wave groups with a target wave height of 12 m and peak periods of $T = 8$, 10, 12, and 14 s.

In the short-period cases $T = 8\,s$ and $T = 10\,s$, the numerically obtained free-surface elevation remains slightly below the theoretical target crest height of $12\,m$. The deviation is on the order of the particle spacing and therefore lies within the expected spatial resolution of the SPH formulation. When

The sole responsibility for the content of this document lies with the author(s). It does not necessarily reflect the opinion of the FOD Economy – Directory of Energy, and does not make them responsible for any use that may be made of the information contained therein.

considering an uncertainty band of $\pm dp/2$, the peak elevation is considered as consistent with the intended focused wave height.

For the longer-period cases $T = 12$ s and $T = 14$ s, the free surface elevation closely approaches the target value and remains stable throughout the focusing event. Wave group coherence is preserved during propagation, and the dominant wave energy is successfully delivered to the floating platform. These conditions therefore provide a more reliable representation of the intended extreme wave excitation within the current numerical setup.

Distinct differences in the phase relationship between wave elevation and mooring line tension are observed across the investigated periods. In the $T = 10$ s and $T = 14$ s cases, the peak fairlead tension occurs shortly after the primary focused wave crest. This behavior suggests a relatively direct coupling between the dominant wave-induced platform motion and the mooring response, with limited temporal separation between excitation and maximum tension development.

The $T = 8$ s and $T = 12$ s cases exhibit a pronounced delay between the focused wave crest and the peak fairlead tension. In these cases, the maximum tension is reached closer to the subsequent wave crest rather than immediately following the primary focus event. This delayed response indicates that the mooring system dynamics extend beyond the timescale of a single wave cycle and are influenced by cumulative platform motion and incomplete recovery of the mooring line between successive wave components. For the $T = 8$ s case, the short wave period limits the time available for the mooring line to restore its equilibrium configuration following initial excitation. As a result, multiple consecutive tension peaks are observed within a relatively short time window. This continuous loading pattern suggests an accumulation of dynamic effects, where residual tension and motion from preceding waves influence subsequent response. Although no distinct snap load is identified, such closely spaced tension peaks may have important implications for fatigue damage and need further investigation.

Meanwhile, in the $T = 12$ s and $T = 14$ s cases, the longer wave period provides additional time for mooring line recovery between wave-induced excitations. The reduced excitation frequency allows partial relaxation of axial strain and platform motion, resulting in more isolated tension peaks and a clearer separation between successive loading cycles. This behavior reflects the lower-frequency nature of the excitation and a reduced tendency for cumulative dynamic amplification.

No abrupt snap load event, characterized by a sharp impulsive tension spike following a clear slack–taut transition, is observed in the present simulations. The tension responses remain smooth and embedded within continuous oscillatory envelopes. Numerical damping inherent to the lumped-mass formulation, together with limited resolution of axial stress-wave propagation, may contribute to smoothing rapid re-tensioning and to an underestimation of extreme peak tension.

The observed sensitivity to wave period highlights the importance of steep, short-period wave conditions in snap load assessment. High-frequency steep waves promote limited recovery time and cumulative mooring response, which may increase the likelihood of slack–taut transitions under specific mooring configurations or excitation strategies. These conditions therefore represent a critical target for further investigation of snap loading under extreme sea states.

At the same time, accurate representation of such steep focused waves requires careful validation of SPH spatial resolution. For short-period cases such as $T = 8$ s, particle spacing must be selected to ensure adequate preservation of wave energy and to avoid resolution-related effects that could mask physically relevant load mechanisms.

6 Conclusion

This study established a numerical setup for simulating the interaction between a semi-submersible FOWT and extreme crest-focused waves using the coupled DualSPHysics–MoorDyn+ model in intermediate water depth. The sensitivity studies showed that the selected resolution, $dp = 0.75\,m$, is

The sole responsibility for the content of this document lies with the author(s). It does not necessarily reflect the opinion of the FOD Economy – Directory of Energy, and does not make them responsible for any use that may be made of the information contained therein.

sufficient to reproduce the overall phase evolution of the focused wave group and a crest height close to the New Wave prediction. The mooring discretization of 180 segments per line was found to provide fairlead tension results almost same with the 400-segment benchmark simulation.

These results indicate that the present numerical setup is suitable for investigating the overall wave–platform–mooring response under extreme focused-wave conditions in intermediate water depth. In particular, the model is able to reproduce the main characteristics of the focused-wave excitation and the corresponding fairlead tension evolution, including the phase difference between wave elevation and mooring response under different peak periods.

Meanwhile, the validation study also showed that the platform free-decay response is not yet fully captured, since stronger damping and some period discrepancy remain relative to the OC4 reference case. Short-period focused waves are more sensitive to spatial resolution, and the lumped-mass mooring formulation may smooth rapid axial transients. Therefore, the present model should be regarded as a validated baseline numerical setup for studying general response trends and identifying critical conditions for further investigation, rather than as a fully validated tool for predicting mooring behaviour in intermediate water depth under extreme conditions. Further refinement of the platform-motion accuracy and additional assessment of the mooring-model limitations are still required in the next stage of this work.

Acknowledgements

This research has been conducted in the framework of the BEL-Float project, which is an Energy Transition Fund project financed by the Belgian FPS Economy.

References

[1] E. E. Bachynski and T. Moan, “Design considerations for tension leg platform wind turbines,” Marine Structures, vol. 29, pp. 89–114, 2012.

[2] O. M. Faltinsen, Sea Loads on Ships and Offshore Structures. Cambridge, UK: Cambridge University Press, 1990.

[3] T. Sarpkaya and M. Isaacson, Mechanics of Wave Forces on Offshore Structures. New York, USA: Van Nostrand Reinhold, 1981.

[4] S. K. Chakrabarti, Hydrodynamics of Offshore Structures. Computational Mechanics, 1987.

[5] J. M. Niedzwecki and S. K. Thampi, “Snap loading of marine cable systems,” Applied Ocean Research, vol. 13, pp. 2–11, 1991.

[6] J. E. Goeller and P. A. Laura, “Analytical and experimental study of the dynamic response of segmented cable systems,” Journal of Sound and Vibration, vol. 18, no. 3, pp. 311–324, 1971.

[7] N. C. Perkins, “Modal interactions in the non-linear response of elastic cables under parametric/external excitation,” International Journal of Non-Linear Mechanics, vol. 27, no. 2, pp. 233–250, 1992.

[8] D. Qiao, J. Yan, H. Liang, D. Ning, B. Li, and J. Ou, “Analysis on snap load characteristics of mooring line in slack–taut process,” Ocean Engineering, vol. 196, p. 106807, 2020.

[9] J. Chen, Z. Yin, C. Zheng, and Y. Li, “Sensitivity analysis of mooring chain fatigue of floating offshore wind turbines in shallow water,” Journal of Marine Science and Engineering, vol. 12, no. 10, p. 1807, 2024.

[10] W.-t. Hsu, K. P. Thiagarajan, M. Hall, M. MacNicoll, and R. Akers, “Snap loads on mooring lines of a floating offshore wind turbine structure,” in Proceedings of the ASME 2014 33rd International Conference on Ocean, Offshore and Arctic Engineering, OMAE2014, (San Francisco, CA, USA), ASME, June 2014.

[11] A. F. L. Governo, J. C. C. Henriques, and L. M. C. Gato, “Modelling mooring line snap loads using a high-order finite-volume approach,” Ocean Engineering, vol. 275, p. 113803, 2023.

[12] M. Hall and A. Goupee, “Validation of a lumped-mass mooring line model with DeepCwind semisubmersible model test data,” Ocean Engineering, vol. 104, pp. 590–603, 2015.

The sole responsibility for the content of this document lies with the author(s). It does not necessarily reflect the opinion of the FOD Economy – Directory of Energy, and does not make them responsible for any use that may be made of the information contained therein.

[13] M. A. Jordán and R. Beltrán-Aguedo, “Nonlinear identification of mooring lines in dynamic operation of floating structures,” Ocean Engineering, vol. 31, no. 3–4, pp. 455–482, 2004.

[14] R. Shi, S. Zhang, X. Liu, and C. Tian, “Modeling and numerical simulation of semitensioned mooring line under taut-slack state,” Shock and Vibration, vol. 2023, p. 7665880, 2023.

[15] J. J. Monaghan, “Smoothed particle hydrodynamics,” Annual Review of Astronomy and Astrophysics, vol. 30, pp. 543–574, 1992.

[16] H. Gotoh and A. Khayyer, “Current achievements and future perspectives for projection-based particle methods with applications in ocean engineering,” Journal of Ocean Engineering and Marine Energy, vol. 2, pp. 251–278, 2016.

[17] A. J. C. Crespo, J. M. Domínguez, B. D. Rogers, M. Gómez-Gesteira, S. Longshaw, R. Canelas, R. Vacondio, A. Barreiro, and O. García-Feal, “Dualsphysics: Open-source parallel cfd solver based on smoothed particle hydrodynamics (sph),” Computer Physics Communications, vol. 187, pp. 204–216, 2015.

[18] J. M. Domínguez, G. Fourtakas, C. Altomare, A. J. C. Crespo, A. Tafuni, and M. Gómez-Gesteira, “Dualsphysics: from fluid dynamics to multiphysics problems,” Computational Particle Mechanics, vol. 9, pp. 867– 895, 2022.

[19] B. Tagliafierro, M. Karimirad, C. Altomare, M. Göteman, I. Martínez-Estévez, S. Capasso, J. M. Domínguez, G. Viccione, M. Gómez-Gesteira, and A. J. C. Crespo, “Numerical validations and investigation of a semi- submersible floating offshore wind turbine platform interacting with ocean waves using an sph framework,” Applied Ocean Research, vol. 141, p. 103757, 2023.

[20] DualSPHysics Development Team, “DualSPHysics Wiki: 3. SPH formulation.” https://github.com/DualSPHysics/DualSPHysics/wiki/3.-SPH-formulation, 2023. Accessed: 2026-03-25.

[21] J. M. Domínguez, A. J. Crespo, M. Hall, C. Altomare, M. Wu, V. Stratigaki, P. Troch, L. Cappietti, and M. Gómez-Gesteira, “Sph simulation of floating structures with moorings,” Coastal Engineering, vol. 153, p. 103560, 2019.

[22] M. Hall, “Moordyn user’s guide,” tech. rep., University of Victoria / NREL OpenFAST community, 2015. User documentation for the MoorDyn lumped-mass mooring dynamics model.

[23] M. Hall et al., “Moordyn v2: New capabilities in mooring system components and load cases,” Tech. Rep. NREL/TP-5000-76555, National Renewable Energy Laboratory, 2020.

[24] A. Robertson, J. Jonkman, M. Masciola, H. Song, A. Goupee, A. Coulling, and C. Luan, “Definition of the semisubmersible floating system for phase ii of oc4,” Tech. Rep. NREL/TP-5000-60601, National Renewable Energy Laboratory (NREL), Golden, CO, 2014.

[25] C. N. Whittaker, C. J. Fitzgerald, A. C. Raby, P. H. Taylor, J. Orszaghova, and A. G. L. Borthwick, “Optimisation of focused wave group runup on a plane beach,” Coastal Engineering, vol. 121, pp. 44–55, 2017.

The sole responsibility for the content of this document lies with the author(s). It does not necessarily reflect the opinion of the FOD Economy – Directory of Energy, and does not make them responsible for any use that may be made of the information contained therein.